1 'robabilistic Analysis of' Ion Engine Accelerator Grid Life

J.E. Polk*, N.R. Moore†, J.R. Brophy‡, L.E. Newlin†, and D.H. Ebbeler†
Jet Propulsion Labor atory
Californ ia Institut e of Techn ology
Pasadena, Ca liforn ia

Abstract

The accelerator grid in two-grid ion optics systems is subject to sputter erosion by charge-exchange ions created in the ion b eam. One poter ntial engine failure mode is accelerator grid structural collapse due to wear. A probabilistic model of accelerator grid service life in which uncertainties about input parameters are treated quantitively reveals that service life with acceptable failure risk is shorter than deterministic analysis using nominal parameter values suggest. The NASA 30-c m ion e ngine with molyb denum grids has a very short service life at 4.65 kWe input power, although derating the thruster to 2.3 kWe or using carbon grid materials can significantly i ncrease life. Uncertainties about the eroded geon etry at failure, the net sputter yield and the impingement ion current in space are the primary risk drivers. Efforts to acquire more information about these drivers and design improvements that decrease the sputter erosion and the required service life have been init - ated.

Introduction

Because of their high specific impulse and high efficiency, ion engines offer significant savings in spacecraft m ass a nd, in cert ain cases, trip time. They are being considered f o r use in a number of earth orbital applications including stat ionkeeping, orbit-raising and repositioning as well as in planetary missions. However, because they arc low thrust devices, very long periods of operation arc required to achieve useful total impulses. During a typical mission an ion engine would be required to operate reliably for thousands of hours. The primary failure mechanism identified in two-grid ion systems is sput ter erosion of the downstream grid by ion impingement. A description of the physical process involved in grid erosion, a general approach to assessing service life probabilistically, and an application o f this approach t o ion engine accelerator (accel) grid erosion are presented in the following.

Accelerator Grid Erosion Phenomena

A diagram of the electrode system in a two-grid ion thruster is shown in Fig. (1). Discharge ions produced upstream are drawn through a sheath t hat forms at the entrance to the apertures in the screen grid and arc accelerated by an axial electric field in the inter-electrode gap. A radial electric field in this region focusses the individual ion beamlets. The accelerator grid is biased negative relative to the ambient space plasma potential to prevent electrons that neutralize the primary ion beam downstream o f the engine from backstreaming int o the discharge chamber. This creates a negative poter ntial well which decelerates the primary ion beamlets. The beamlets are a lso subject to radial electric fields in this region which c ause them to diverge.

The accel grid may be impacted d irectly by primary beam ions, although this source of impingement current ca n be practically eliminated by proper design and operation of the ion optics. In addition, the accel grid collects s l o w ions generated from neutral gas in the interelectrode gap and downstream of the grid. In space, the engine is the only source of neutral

*Technical Group Leader
†Member of the Technical Staff
‡Group Supervisor

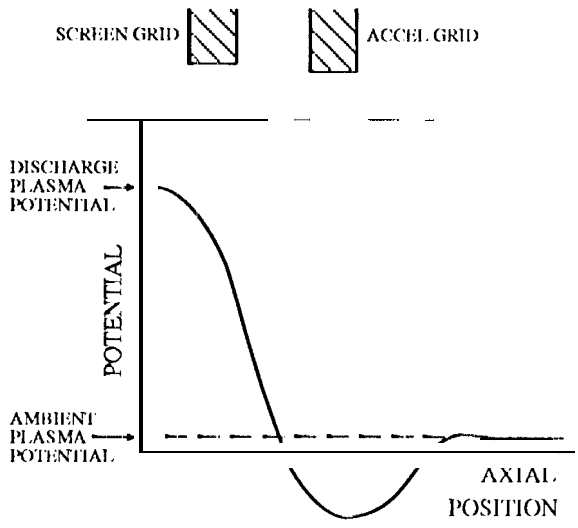

Figure 1: Diagram of two-grid electrode system and axial potential distribution.

gas. An inevitable consequence of propellant utilization inefficiencies is the leakage of neutral atoms from the discharge chamber, although the density of these source atoms drops rapidly downstream of the grid [1]. In ground test facilities a second population of ambient gas atoms can exist with a more or less uniform distribution and a density determined by the engine propellant flow rate and the pumping capability of the facility.

These neutrals can be ionized either by collisions with electrons produced by the neutralizer cathode or in charge-exchange collisions with primary beam ions. In charge exchange collisions a thermal neutral atom surrenders an electron which recombines with a high speed ion. This creates a high velocity neutral atom that escapes with the beam and a thermal ion. Order of magnitude analyses and experiments indicate that the contribution from electron-impact ionization is small compared to that from charge exchange processes [1].

The majority of charge exchange ions created in the deceleration zone downstream of the accel grid do not have sufficient energy to escape from the potential well and are therefore drawn to the accel grid. Experiments and particle simulations indicate the existence of a slight potential hump downstream of the deceleration zone in the beamlets. In contrast, the potential appears to decrease monotonically toward the accel grid between adjacent beamlets [1,2]. Therefore, a fraction of the slow ions generated in the weak electric field downstream of the neutralization plane can be collected if their velocity is back toward the grid when they are created. In space, most of the neutrals emitted from the discharge chamber have velocities directed away from the grids, so very few of the charge exchange ions created downstream of the deceleration zone will be collected [3]. In addition, the density decreases rapidly in the axial direction, so fewer ions are generated downstream. However, in ground test facilities the ambient neutrals have an isotropic velocity distribution and a significant quantity of the ions created downstream will impinge on the accel grid. In fact, the charge exchange ions generated from the background gas appear to dominate the impingement current in ground-based tests [3,1].

The impingement ions follow trajectories that are dictated by their origin and the structure of the potential near the grid. Particle simulations show that most of the ions impinge on the downstream face of the electrode and are focussed into the central part of the webbing between holes by the radial electric fields of adjacent beamlets [2,4]. The characteristic erosion pattern observed on the downstream face of the accel grid in long duration tests reveals the damage caused by the impingement ions. The photograph in Fig. (2), taken after a long duration test described in [5], shows a series of grooves between holes forming a hexagonal pattern with deeper pits at the intersection points between three holes where the impingement current density peaks.

The mass loss in the pits and grooves is caused by sputtering, a collisional process in which incident ions can eject surface atoms. Sputtering occurs only when the incident ion energy exceeds a certain threshold and sufficient energy is transferred in the collision to overcome the surface binding forces. At energies near the threshold the ejected atoms are usually directly involved in collisions with the incident ion, although at higher energies they may be part of a collision cascade initiated by the incident ion.

Sputtering is characterized by the yield, which is defined as the expected number of atoms ejected per incident ion. The yield is a function of the ion en-

Figure 2: Photograph showing the characteristic form of accel grid erosion. (see back)

ergy, the masses of the ions and target atoms, the surface binding energy and the incident angle, reaching a maximum value at a particular oblique angle [6]. It does not generally depend on the current density, but is a function of the total dose. This is primarily due to changes in the geometry as the grid wears. Initially the impingement ions are normally incident on a flat surface, and most of the sputtered atoms escape. As the grooves form, the incident angle may increase, causing the absolute yield to rise. However, redeposition of sputtered atoms in the groove can reduce the net yield [7]. As the pits and grooves penetrate the accel grid, sputtered atoms can escape upstream through the grid, as well as downstream.

When the pits wear completely through the grid, the ions incident in that region are either reflected in the interelectrode gap and strike the upstream face or are focussed along the channels. Grid penetration then proceeds along the channels as shown in Fig. (2) until complete structural failure occurs. Loss of grid structural integrity as a result of sputter erosion in the characteristic hexagonal groove pattern is one potential failure mechanism. Loss of strength caused by grid erosion can cause shorts as individual ringlets or sections of the accel grid collapse and bridge the interelectrode gap under the electrostatic stresses. Even if shorts are avoided, it becomes impossible to properly focus the primary ions and prevent electron backstreaming as large holes in the grid form.

Accelerator grid sputter erosion can be minimized by proper environmental conditions and thruster operation, but is unavoidable at some level. Uncertainty in our description of the physical processes of grid erosion in addition to their intrinsic variability makes it impossible to calculate grid life exactly. Relying on extensive testing to characterize grid life with high confidence would be prohibitively costly and time-consuming. It is therefore useful to model accelerator grid erosion probabilistically, using available information from tests and knowledge of the physical processes that lead to failure.

Probabilistic Service Life Assessment

In the assessment of accel grid service life presented here, test information and analytical models are used in a statistical structure in which uncertainties about failure prediction are quantitatively treated. This probabilistic analysis can be performed with the information available at any particular time to obtain a probabilistic estimate of service life that is warranted by what is known about a failure mode at that time. This probabilistic method is applicable to failure modes which can be described by analytical models of the failure phenomena, even when such models are uncertain or approximate.

By conducting service life sensitivity analyses probabilistically, sources of unacceptable failure risk can be identified and corrective action can be delineated. Design revision, additional characterization of environments, improvement of analytical model accuracy, and improved characterization of material behavior are among the options for controlling risk that can be quantitatively evaluated by probabilistic sensitivity analyses. Using sensitivity analysis results, test and analysis programs focused on acquiring information about the most important risk drivers can be defined, enabling limited financial resources to be allocated more effectively to achieve life goals.

Probabilistic service life assessment can be employed in the design and development process to avoid

Figure 3: Probabilistic failure risk assessment.

(See bid_.)

compounding design conservatisms and margins that unnecessarily increase cost or weight. Probabilistic analysis is of particular value when uncertainties exist about important governing parameters or when design conservatism and redundancy used in the past must be reduced to meet more stringent cost, weight, or performance requirements.

Information from test or service experience can be combined with information from analytical modeling to estimate failure risk quantitatively using the approach shown in Fig. (3). Probabilistic failure modeling is based on available knowledge of the failure phenomenon and of such governing parameters as ion impingement current and sputtering yield. The prior failure risk distribution of Figures (3) and (4) is derived from probabilistic failure modeling. This prior distribution can be modified to reflect available sacccss/failure data in a Bayesian statistical analysis. The probabilistic service life assessment approach shown in Figures (3) and (4) is discussed in detail by Mom, et al. [8,9, II 0].

Experience includes physical parameter in formation in addition 10 success'failure data. Information about physical parameters can be derived from measurements taken during tests or service, from analyses to bound or characterize parameter values, from applicable experience with sin ilar syst ems, or from laboratory tests. Measurements of physical parameters used in analytical modeling, e.g., grid impingement current or eroded area, can be an important information source in failure risk assessment. Physical parameter information is incorporated into probabilistic failure modeling and is reflected in the prior failure risk distribution.

Figure 4: Probabilistic failure modeling.

(See back)

Success/faillIrc data can be acquired from life testing or service experience. The failure risk distribution resulting from the combination of the prior distribution and the success/failure data is the description of failure risk which is warranted by the information availa ble. As additional information regardin g governing physical parameters becomes availa ble it can be incorporated into analytical modeling to obtain a revised prior failure risk distribution. Additional information in the form of success/failure data can be processed by the Bayesian statistical analysis of Fig. (3) to update the prior failure risk distribution using the procedure given by Moore, et al. [10,1 1]. However, as would be expected, a few successful life demonstrations will not affect a prior distribution with which they are consistent.

The analysis procedures used in probabilistic failure modeling, shown in Fig. (4), are directly derived from deterministic methods for analyses of grid service life. The accuracy of the models and procedures used in probabilistic failure modeling should be probabilistically described and treated as a driver.

A driver for which uncertainty is to be considered must be characterized by a probability distribution over the range of values it can assume. That distri-

bution expresses uncertainty regarding specific driver values within the range of possible values. A driver probability distribution must represent both intrinsic variability of the driver and uncertain knowledge or limited information on which to base the driver characterization.

Stochastic drivers are characterized by using the information that exists at the time of analysis. If driver information is sparse, the probabilistic characterization of such a driver must reflect that sparseness. If extensive experimental measurements have been performed for a driver, its nominal value and characterization of its variability can be inferred directly from empirical data. However, if little or no directly applicable empirical data is available, analysis to characterize a driver or experience with similar or related systems must be used. Driver distributions must not overstate the precision implied by the available information.

Some general guidelines for characterizing stochastic drivers have emerged from case studies conducted to date as given in Moore, et al. [9,8,11]. For drivers which have physical bounds, such as controlled dimensions or parameters with physical upper limits, the Beta distribution parameterized with location, shape, and scale parameters has been successfully used. If only bounds are known, a Uniform distribution is appropriate. For a driver whose variation can be thought of as due to the combined influence of a large number of small independent effects, the Normal distribution can be used. Past experience in characterizing a particular driver such as a material property may suggest the use of a particular distribution, for example, Weibull, Normal, or Lognormal.

A hyperparametric structure for driver distributions has been found useful in describing available information about a driver. For example, to characterize a driver, information from engineering analysis might be used to establish upper and lower bounds. In order to capture the fact that the mean value may not be known with certainty, the mean value may be represented by a Uniform distribution between the upper and lower bounds. This Uniform distribution is the hyperdistribution associated uncertainty about the true mean value, and its parameters are the associated hyperparameters.

Monte Carlo simulation has been used as the principal computational method in probabilistic failure modeling because it is a general method that can be used with failure models of any complexity. Continually increasing computer power due to improving hardware and software is steadily expanding the practical application of Monte Carlo simulation. Efficient Monte Carlo techniques can be used to reduce the number of simulation trials when computational time is an issue. Certain analysis methods such as plasma particle simulation models, may be too computationally intensive for practical use in Monte Carlo simulation. However, the output of these models can be represented as response surfaces over the range of variation of significant parameters, see Moore, et al. [8,10]. The uncertainties of response surface representations must be treated as drivers if significant.

Alternative computational methods, for example, FORM/SORM, see Madsen, et al. [12], may fail to give accurate results for problems in which significantly nonlinear models are employed and driver uncertainty is large. Computational methods are discussed further by Moore, et al. [11,10].

Accelerator Grid Erosion Analysis

The deterministic erosion model used in this analysis describes the mass loss due to ion sputtering and is imbedded the Monte Carlo simulation procedure outlined in Fig. (5). This model expresses the time to initial structural failure of the grid as a function of drivers which may be either deterministic or stochastic. The drivers consist of geometry, current and accel grid voltage, material properties and accuracy factors which account for uncertainties in the analysis.

A basic structural unit of the grid can be defined by the triangular region shown in Fig. (6). End of life is defined as the point at which the first structural unit is divided in two by erosion in the central channel. This will generally occur first in the center of the grid where the erosion rate is the highest. This failure criterion can be expressed quantitatively in terms of the fractional mass loss in the structural unit by the relationship

$$\left(\frac{M_e}{M_{su}}\right) = \left(\frac{M_e}{M_{su}}\right)_f, \qquad (1)$$

where M_e is the eroded mass in the channel, and M_{su} is the initial mass of the structural unit,

$$M_{su} = \rho_g A_{su} t, \qquad (2)$$

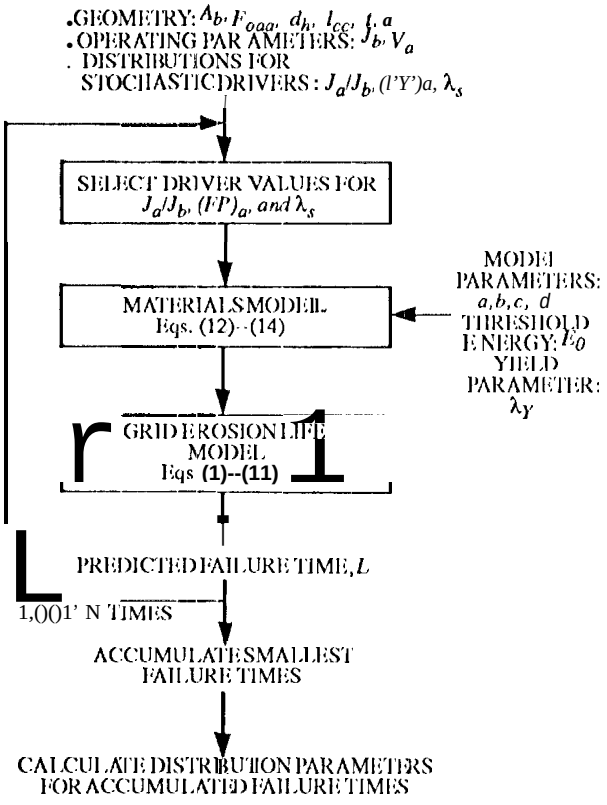

Figure 5: Sputter erosion failure simulation.

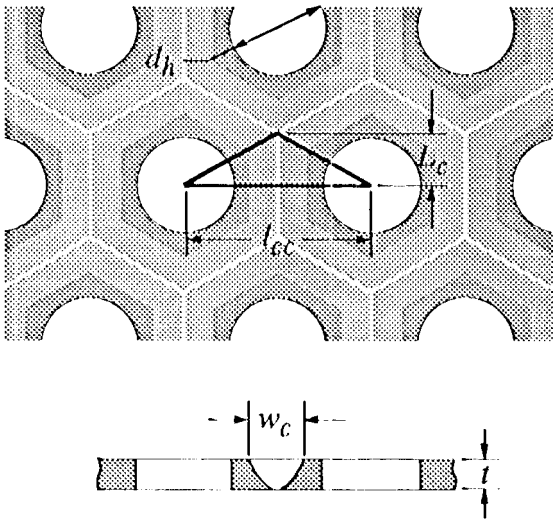

Figure 6: The basic structural unit and the model of groove geometry at failure.

in which ρ_g represents the density of the grid material, A_{su} is the initial structural unit webbing area and t is the initial grid thickness. The webbing area is given by the expression

$$A_{su} = \frac{\sqrt{3}}{12} l_{cc}^2 - \frac{\pi d_h^2}{24}, \qquad (3)$$

where l_{cc} is the center-to-center hole spacing and d_h is the hole diameter. The parameter $(M_e/M_{su})_f$ is the allowable fractional mass loss before the unit is cut in two, and is a function of the grid geometry and the geometry of the channel at failure.

The fractional mass loss averaged over a structural unit after a cumulative operating time τ due to sputtering from singly charged ions is given by the expression

$$\left(\frac{M_e}{M_{su}}\right) = \frac{J_{a,su}\,\tau\,Y_{net}\,m_g}{e M_{su}}, \qquad (4)$$

where $J_{a,su}$ is the average ion impingement current in the structural unit, Y_{net} is the average net sputter yield in atoms per incident ion, m_g is the mass per atom of grid material and $e = 1.6 \times 10^{-19}$ C is the fundamental electron charge. These two equations define the time to structural failure, given proper specification of the drivers: grid geometry, geometry of the channel at failure, impingement current $J_{a,su}$ and the net sputter yield Y_{net}.

Although there have been significant advances in modeling the local distribution of impingement ion flux and energy in the erosion pattern using particle simulation methods [2,3], these codes are too computationally intensive to include in the failure simulation. The failure model has therefore been expressed as approximate relationships in terms of observable parameters averaged over the structural unit.

The failure criterion can be defined by the expression

$$\left(\frac{M_c}{M_{su}}\right)_f \approx \frac{l_c A_c}{t A_{su}}, \tag{5}$$

where A_c represents the cross-sectional area of a channel which just divides the structural unit. This channel shape is assumed to be constant along the the length l_c, as shown in Fig. (6). The effective channel length is approximated by

$$l_c = \frac{\sqrt{3}}{6} l_{cc}. \tag{6}$$

Use of this approximation slightly overestimates the mass lost at the apex of the structural unit from a channel of uniform cross-section. This is not expected to significantly bias the life calculations, because in practice much of the impingement ion current generated by three adjacent beamlets is focused into the central region (the intersection of the channels bisecting the three structural units) and causes more severe erosion than in the rest of the channels. The channel cross-sectional area is modeled as

$$A_c = \frac{2}{3} \lambda_s w_c t, \tag{7}$$

where w_c is the width of the channel at the downstream surface. This expression represents a parabolic cross-section modified by the shape factor λ_s, which describes uncertainty about the channel shape. The channel width can be expressed in the form

$$w_c = l_{cc} + (l_{cc}^2 - 12\alpha A_{su}/\sqrt{3})^{1/2}, \tag{8}$$

where $\alpha = A_c/A_{su}$ is the eroded area fraction, the projected area of the erosion groove A_c compared to the structural unit webbing area. Equations (2) to (8) permit the failure criterion in Eq. (1) to be expressed in terms of the grid geometry parameters d_h, t and l_{cc} and the channel shape parameters α and λ_s.

The current in the structural unit in the center of the **grid** (which **is** subject to the highest impingement current) can be expressed as the product of the structural unit area and the average local impingement current density $j_{a,peak}$ (ignoring local current density variations due to the discrete ion beamlets),

$$J_{a,su} = j_{a,peak} A_{su} = \left(\frac{J_a}{J_b}\right) \frac{J_b A_{su}}{A_b(1 - F_{oaa})(FP)_a}. \tag{9}$$

where J_a/J_b is the ratio of total impingement current to beam current, A_b is the active beam area, F_{oaa} is the open area fraction of the accel grid and the impingement current density flatness parameter is defined as

$$(FP)_a = \frac{J_a}{A_b(1 - F_{oaa}) j_{a,peak}}. \tag{10}$$

The impingement current density flatness parameter can be equated to the flatness parameter describing the beam current density distribution,

$$(FP)_a = (FP)_b, \tag{11}$$

if the ratio of local average current densities (j_a/j_b) is constant over the entire grid. The assumption that j_a is proportional to j_b locally is valid for charge exchange ions if they strike the accel grid at radial and azimuthal positions close to those where they were created. This should be satisfied in space, where the impingement ions originate inside the deceleration region and the local electric fields guarantee that they intercept the grid near their point of origin. In ground test facilities, however, the majority of the impingement ions are created downstream of the neutralization plane and may drift to radial and azimuthal locations very different from where they were created before being captured by the accel grid. This has the effect of making (If '}'). somewhat larger than $(FP)_b$. The assumption that the constant of proportionality between j_a and j_b dots not vary over the grid is accurate only if the axial neutral density profile and the effective length from which charge exchange ions are drawn do not vary with radial position.

The average net sputter yield is assumed to be proportional to the yield at normal incidence,

$$Y_{net} = \lambda_Y Y_{\theta=0}, \tag{12}$$

where λ_Y is a stochastic factor representing variations of the average net yield from the yield at normal incidence due to dose effects (primarily redeposition of sputtered material and oblique incidence of bombarding ions). The available yield data for krypton and xenon incident 011 molybdenum and carbon can be fit well with an empirical relationship of the form

$$Y_{\theta=0} = aE_i^b \left(1 - \frac{E_0}{E_i}\right)^c \left(1 + \frac{m_i E_0}{E_i}\right)^d, \quad (13)$$

where E_i is the incident ion energy, E_0 is the threshold for sputtering, and m_i is the atomic mass of the incident ion. The first term accounts for variation with ion energy, while the second term reproduces the threshold behavior. The final term represents the variation in yield with bombarding species mass. The parameters a, b, c and d can be estimated from the data for sputtering yield as a function of incidention energy and mass. In calculating accel grid life, the incident ion energy is given by the relationship,

$$E_i = eV_a, \quad (14)$$

where it has been assumed that all of the ionsstrike the grid with the maximum possible energy, given by the accel grid potential V_a. This is appropriate for testing in ground-based facilities where most of the impingement ions originate outside of the potential well surrounding the accel grid, but is a conservative assumption for space conditions where many of the ions created inside the deceleration zone will not fall through the entire potential.

With the equations discussed above, the complete model of grid life can be represented in terms of the geometry drivers $d_h, l_{cc}, F_{oaa}, A_b$ and et, the drivers representing operating conditions $(J_a/J_b), J_b, (FP)_b$ and V_a, the material properties a, 6, c, d, E_0, ρ_g, m_g and m_i, and the drivers characterizing model uncertainty λ_s and λ_Y.

Calculations of Accelerator Grid Life

Four test cases were examined using the model presented above. The deterministic model of grid life was used to calculate the time to failure for the input parameter values listed in column 2 of Table (). These values correspond to the geometry, operating conditions and material properties for the endurance test described in [5] in which a 30 cm two grid ion engine was operated until grid failure under accelerated test conditions. The full probabilistic model was used to assess the lifetime of the accel grid in the 30 cm ring-cusp thruster [13,14], which is currently baselined for use in the NASA SEP (Solar Electric Propulsion) Technology Applications Readiness (NSTAR) program, a NASA-sponsored experiment 011 the Air Force Space Track and Autonomous Reposition (STAR) mission. The failure probability was calculated for conventional molybdenum optics at 4,65 kWe engine power (5 kWe power input to the power processing unit) and at 2.3 kWe (2.5 kWe total power), the design point for the NSTAR experiment. The 4.65 kWe condition was then reexamined assuming the use of carbon as the grid material. Graphite, carbon-carbon composites and diamond are now being considered as advanced grid materials because of superior sputter resistance [15,16,17,18,19]. The driver distributions used in these analyses are also shown in Table (). In this section a detailed description of the driver characterization will be followed by a discussion of the calculated lifetime distributions and the analyses performed to determine the driver sensitivity.

Specification of Driver Distributions

The initial grid geometry is specified by the hole diameter, center-to center spacing, open area fraction, beam area and grid thickness. These parameters were assigned the fixed values given in Table ().

The channel geometry at failure is described by the eroded area fraction and the shape factor. The eroded area fraction is fundamentally determined by the ion trajectories, and examination of the grid used in the test-to-failure [5] suggests that the eroded area fraction does not change significantly with time (i.e. ion dose or geometry). Therefore the erosion patterns observed in relative short duration tests can be **used** to estimate this parameter. The results of eroded area fraction measurements 011 a number of accel grids used in endurance tests performed with a variety of propellants, operating conditions and geometries are summarized in Table (). The values range from approximately 0.4 to 0.55. These data and the current understanding of the phenomena that dictate the eroded area fraction do not provide suf-

	Case 1	Case 2	Case 3	Case 4
Geometry				
A_b (cm^2)	658.7	658.7	658.7	658.7
F_{oaa}	.242	.242	.242	.242
d_h (11111))	**1.14**	*1.14*	*1.14*	*1.14*
l_{cc} (mm)	2.21	2.21	2.21	2.21
t (mm)	0.360	0.508	0.508	0.508
α	*0.50*	Parametric (0.2, 0.6)		
λ_s	*1.31*	U(1.0, 1.5)		
Operating Conditions				
Power(kWe)	?	4.65	2.3	4.65
J_a/J_b	*0.013*	Be(0, *0.003, 0.73, 6.6)*		
(1''1')"	*0.71*	U(0.4, 0.6)		
J_b (A)	2.7	3.0	1.8	3.0
V_a (\')	510	300	150	*300*
Material Properties				
Propellant/Grid	Kr/Mo	Xe/Mo	Xe/Mo	Xe/C
V_0 (CV)	43	48	48	111
a	0.0414	*0.0414*	*0.0414*	4.257× 10-4
b	0.5655	0.5655	0.5655	1
c	3.2102	3.2102	*3.2102*	1
d	-0.0431	-0.0431	-0.0431	0
λ_Y	1	1	1	1

Table 1: Driver values used in test cases,

ficient information to identify parameters 011 which this driver depends or to specify a range applicable to space operation. It was therefore treated parametrically in the probabilistic calculations, at values ranging from 0.2 to 0.6. The minimum value observed experimentally, 0.4, was used as the nominal value.

Detailed examination of the test-to-failure grid [5] confirms that the channels do maintain an approximately parabolic shape (altl rougl r with rou nded edges) as they progress int o the grid. However, after penetration of the grid occurs, undercutting by ions reflected in the interelectrode gap and further erosion of tl ie walls results in an increase in the average cross-sect ional area of the channels. These effects are estimated to cause up to 50 percent more mass l 0 s s than if the channels had a uniform parabolic cross-section. Therefore, λ_s was represented as a uniform distribution over the range (1 .0,1 .5),

The engine operating parameters that affect accel grid life are the beam current, accel grid voltage, the ratio of impingement current to beam current and the flatness parameter. The beam current and grid voltage were fixed at the values show n in Table (), since there exists no significant variability or uncertainty regarding their values. The probabilistic calculations were performed for engine operation in space, and the ratio of impingement current to beam current was chosen to reflect this. The impingement current measured in ground tests with noble gas propellants is not applicable to conditions in space due to higher tank pressures. Mercury data is expected to be representative of that found with xenon in space because the propellant utilization efficiency and charge exchange cross sections arc similar for these propellants in optimized engines and at operating conditions considered in this analysis [13]. The impingement current fraction was characterized on the basis of data from 30 cm thrusters at low back pressures with mercury a s

	Ref. [5]	Ref. [13]	Ref. [?]	Ref. [?]
Propellant/Grid	Kr/Mo	Xe/Mo	Hg, Xe/Mo	Hg, Xe/Mo
Tank Pressure (Pa)	3.4-4.1 $\times 10^{-4}$	1.7 X10-3	1.9×10^{-3} (Xe)	8.6×10^{-5} (Hg)
V_a (V)	510	331	510 (Xe)	308 (Hg)
J_b (A)	2.8	3.19	5.0 (Xe)	2.0 (Hg)
J_a (mA)	35	17.4	47 (Xe)	5 (Hg)
Test Duration (hrs)	633	900	567 (Xe)	$\approx$ 6200 (Hg)
			5300 (Hg)	$\approx$ 200 (Xe)
d_h (mm)	**1.14**	**1.14**	1.52	1.14
l_{cc} (111111)	**2.21**	2.21	2.21	2.21
w_c (111111)	**0.47**	**0.37**	0.37	0.43
α	0.50	0.40	0.54	0.46

Table 2: Measured values of eroded area fraction.

the propellant. The impingement current fractions measured in [20] were specified by a Beta distribution ranging from a lower bound of zero to an upper bound of 0.3 percent.

The flatness parameter used in this model serves primarily to account for macroscopic nonuniformity in the mass loss distribution across the grid. For the test-to failure the true radial mass loss distribution was determined by sectioning the grid into concentric rings and weighing them. The measured mass loss distribution can be represented by a flatness parameter of about 0.71, which is broader than the expected beam current distribution (with a flatness parameter of about 0.5). As discussed above, this is probably a facility effect caused by the collection of charge exchange ions produced far downstream. This measured value **was** used in the analysis of the test-to-failure grid, but for the probabilistic analyses of 30 cm engine operation in space the impingement current flatness parameter was assumed to equal the beam flatness parameter. This was represented by a uniform distribution over the range (0.4, 0.6). The minimum value was chosen as the lower limit for acceptable engine performance and the maximum value represents a practical limit to the achievable beam flatness.

The materials characterization involves specifying the atomic mass of the propellants and the atomic mass and mass density of the grid materials, as well as the threshold energy, normal yield and yield factor λ_Y that give the sputtering characteristics of the ion-target combinations. For xenon and krypton ions incident on molybdenum, the threshold energy values in [21] were used. No reliable threshold measurements were found for xenon incident on carbon, so the threshold energy for this combination was estimated from the sputtering yield data.

The normal yield parameters a, b, c, and d in the sputtering model, Eq. (13), were estimated using data for krypton and xenon on molybdenum corrected for secondary electron emission [7]. For carbon, there are too few measurements available to estimate all four parameters and the threshold energy. However, the data in [7,22] for xenon on carbon are well represented by a linear model obtained by setting $b = c = 1$ and $d = 0$ in Eq. (13). The samples used in [7] were of an unspecified form of carbon, while those in [22] were pyrolytic graphite cut parallel to the net plane. Because the sputter yield for carbon can vary depending on the type and crystallographic orientation of the material [23], these data may not be representative of all the proposed carbon grid materials. The available yield data appear to be free from systematic biases due to residual chamber gases, multiple ion production, oblique ion incidence and backscattering of sputtered atoms [24,25] and the data exhibit little random variation, so the parameters were given conservative fixed values that guaranteed predicted yields above the measured values in the energy range of interest. The sputtering yields are shown in Fig. (7) and the estimated parameters are given in Table 0.

There is very little information on the extent to which the net sputtering yield can vary from the value

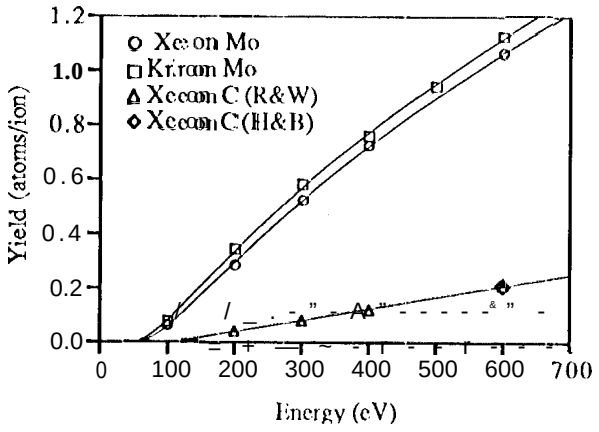

Figure 7: Measured sputter yields and Model fits.

at normal incidence on smooth surfaces, although limited data suggest that it is decreased by surface roughness [7]. The yield factor λ_Y was therefore conservatively set equal to unity.

Results

The test described in [5] was terminated after 633 hours when a flake of sputter-deposited material shorted the two electrodes. Post-test examination of the accelerator grid showed that it was also very near structural failure caused by pits and grooves formed by sputtering. The total mass loss calculated from the initial grid geometry and the mass measured after the test was 62 g. A total mass loss at failure of 62 g is predicted by the model with the same assumptions for the initial grid geometry if a channel shape factor of 1.31 is assumed. The calculated time to failure using the driver values in Table 0 is 510 hours. If intrinsic variability in the normal sputter yield is small and the sputtering factor λ_Y is actually equal to unity, the measured time to failure and that given by the deterministic calculation should be comparable, because all other drivers were measured directly. The discrepancy is indicative of model specification error, which most likely appears in the value chosen for λ_Y. This implies a slight lowering of the net sputter yield due to redeposition of sputtered atoms. A true value of 0.8 for λ_Y is sufficient to explain the discrepancy. If this interpretation is correct, the error associated with $\lambda_Y = 1$ results in conservatism in the probabilistic calculations.

Figures (8), (9) and (10) show the calculated failure distributions for the 30 cm engine with molybdenum grids at 4.65 and 2.3 kWe and with carbon grids at 4.65 kWe. The peak of the curves represents the B50[1] life, and corresponds approximately to the value of life that would be predicted deterministically using the nominal driver values. The uncertainty captured by the stochastic drivers J_a/J_b, $(VP)_b$ and λ_s serves to decrease the accel grid life considerably from that calculated with the nominal values. Deterministic calculations using the nominal driver values can therefore provide a false sense of security, because they do not reveal the impact of uncertainty in assessing service life. The predicted life is also strongly dependent on the chosen value of the eroded area fraction α.

At the 4.65 kWe operating point the 30 cm design with molybdenum grids has insufficient life. With a value of 0.4 for the eroded area fraction a failure probability of 50 percent after only 4070 hours of operation is calculated, and the B.1 life is less than 2100 hours. This nominal value for the eroded area fraction was chosen because it is the lowest observed in the ground-based tests summarized in Table (), but we cannot say with any certainty that it will not be lower in space.

Recognizing the risk associated with operation at 4.65 kWe, the 2.3 kWe operating point was proposed for the NSTAR experiment. As Fig. (9) shows, a combination of lower beam current and lower aced grid voltage at this derated condition results in a factor of five increase in life compared to the 4,65 kWe point. With an eroded area fraction of 0.4 the B50 life is in excess of **20,000** hours and the B.1 life is 10,600 hours.

The impact of advanced grid materials is shown by the life assessment of carbon optics in Fig. (10). A lower sputter yield and higher atom number density result in an order of magnitude increase in life compared to molybdenum grids. Even at the demanding 4.65 kWe operating condition the B.1 life is nearly

[1] A B-life is the value of accumulated operating time to failure at a failure probability specified as a percent; e.g., B).] is the life at a probability of 0.001 or 0.1 percent and B50 is the life at a probability of 0.5 or 50 percent.

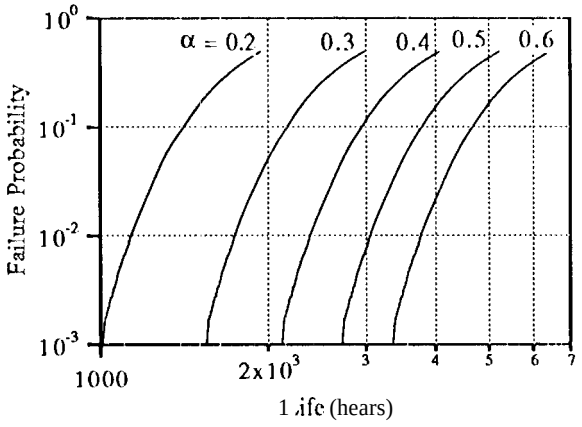

Figure 8: Probabilistic life assessment for operation at 4.65 kWe with Mo grids.

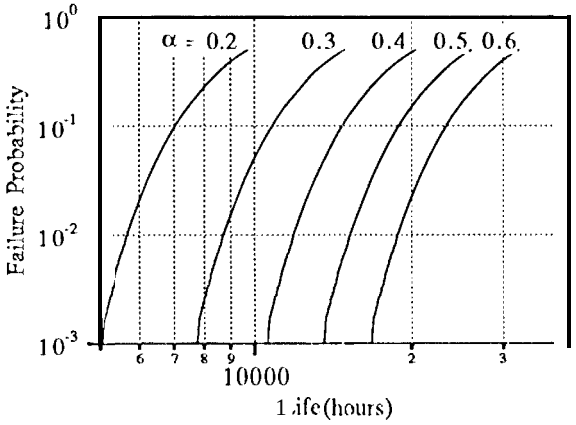

Figure 9: Probabilistic life assessment for operation at 2.3 kWe with Mo grids.

22,()()() hours and the 50 percent failure probability occurs at 42,000 hours.

The parametric study of the eroded area fraction shows **that** it **is** one of the most important drivers in determining accel grid life. An analysis of the sensitivity to the other stochastic drivers was also conducted and is shown for operation with molybdenum grids at 2.3 kWe in Fig. (1 1). In this analysis individual drivers were allowed to vary while the other parameters were held fixed at the nominal values and the results compared with that in which all drivers were allowed to vary. The results show which drivers contribute the most to the reduction in life from the fixed driver case. For the designs considered here, the uncertainty in the impingement current contributes the most to the failure risk, with flatness parameter and channel shape factor playing slightly lesser roles. Sensitivity analyses conducted for the other two cases yielded similar results.

In Fig. (12) the life distribution with variation of all drivers is compared to calculations in which the shape factor λ_s was held fixed at the nominal value and the upper and lower bounds **of** the specified distribution. The curve generated by sampling from a uniform distribution between the two extremes merges with the curve fixed at the nominal value of 1.25 at the B50 point, as expected. For lower values of the failure probability, however, the curves diverge and the Drol)-

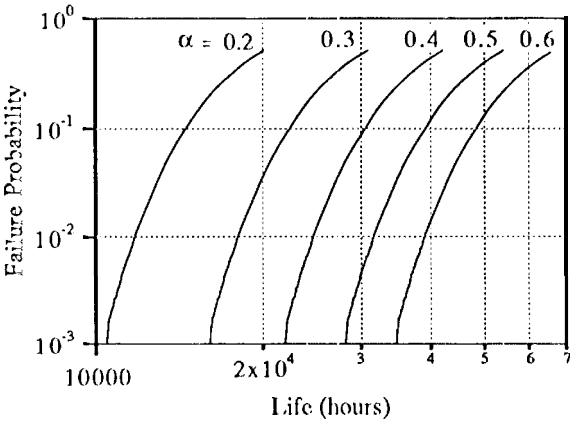

Figure 10: Probabilistic life assessment for operation at 4.65 kWe with C grids.

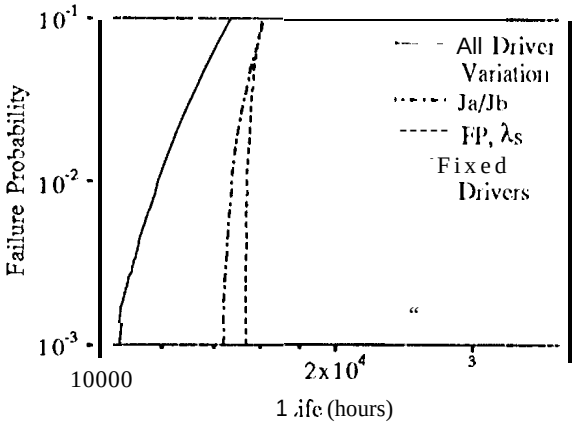

Figure 11: Probabilistic sensitivity analysis for 2.3 kWe operation with Mo grids and an eroded area fraction of 0.4.

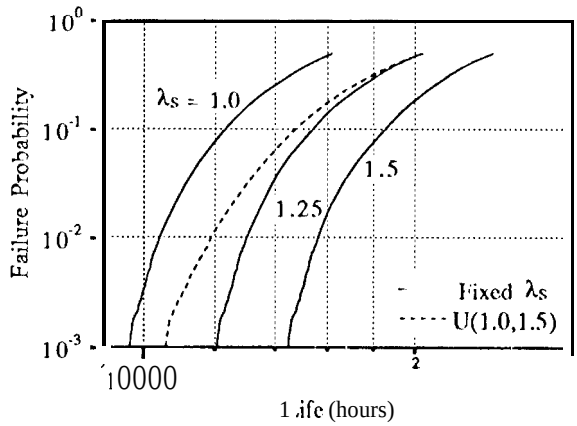

Figure 12: Parametric study of channel shape factor for 2.5 kWe operation with Mo grids (α = 0.4).

abilistic calculation] moves toward lower lives. The left-hand tail of the failure probability distribution is affected by the more conservative portions of the driver distributions.

Approaches to Managing Risk

The probabilistic accel grid service life model clearly demonstrates that the risk is driven by lack of knowledge, particularly with respect to the eroded area fraction α, the sputtering factor λ_Y and the impingement current fraction J_a/J_b. Subsequent activities will be directed toward acquiring more information on these drivers as well as implementing design improvements which reduce the sputter erosion and decrease the required grid service life.

Information Acquisition

A number of experiments involving examination of erosion patterns in thin copper films deposited on a molybdenum accel grid are planned at JPL to determine how the eroded area fraction varies with tank pressure, beam current, accel grid voltage and propellant species. Use of thin films permits determination of the areas subject to the highest impingement current density in relatively short duration tests. In addition, ERC, Inc. will continue the development of plasma simulation codes to predict impingement ion trajectories [3]. The objective of these efforts is to determine bounds on the value of α that can be incorporated in the probabilistic analysis.

A simulation code is also being developed at JPL to track the trajectories of sputtered atoms and the growth of the erosion grooves. This will provide information on the effect of redeposition on the net yield that can be incorporated in the analysis as a probability distribution for the parameter λ_Y. Refinements to the plasma simulation codes developed by ERC, Inc. and further experiments and analytical modeling at Colorado State University [1] should provide additional information on the value of J_a/J_b in space.

In the near future, relative sputter yield measurements will be performed at JPL on samples of molybdenum, graphite, carbon-carbon sheets and diamond films to improve the materials model. Absolute sputter yields may also be measured to supplement the limited database found in the literature.

Technology development for the NSTAR program will also yield additional driver information. For example, further development of the 30 cm ring-cusp thruster at the NASA Lewis Research Center will provide a better characterization of operating parameters such as the beam flatness. In addition, two 2000 hour tests and one 12,000 hour endurance test are planned as part of NSTAR. The 2000 hour tests, to

be conducted in two different facilities with different tank pressures, are too snort to affect failure risk estimates for long duration missions, but will provide valuable information on the operating conditions and erosion patterns and may reveal unanticipated failure modes. The 12,000 hour test will yield additional information on drivers and the success or failure of this test can be used directly to improve the prior distribution.

Design Improvements

The model demonstrates the tremendous potential of improved grid materials. Development or graphite [15], carbon-carbon [16,17,18] and diamond grids [19] is continuing. In addition, screen-accel-negative decel (S AND) three-grid optics are being studied as one approach to reducing sputter erosion [?, 15]. In this optics configuration a third grid located downstream with a negative bias somewhat less in magnitude than that on the accel grid. This electrode then collects most of the charge exchange ions at a low enough energy to avoid rapid sputtering, effectively shielding the accel grid. The accel grid voltage can also be lowered in this configuration, so that the ions that do impinge on it cause less damage.

Use of segmented ion engines is another risk management approach which exploits the throttling requirements of certain mission applications to reduce the grid service life requirements [26,1.5]. In this architecture, four or more ion sources are used with a common neutralizer and power processing unit to form a single engine. Throttling is accomplished by turning off segments, effectively saving them for use later when other segments have reached their design life. Depending on the mission throttling requirements, this approach can result in a significant reduction in the required grid service life.

Conclusions

A probabilistic assessment of accel grid service life incorporating uncertainty about the governing parameters reveals that the service life at an acceptable failure risk is considerably shorter than deterministic calculations suggest. Conventional 30 cm molybdenum grids have very limited life at the 4.65 kWe operating point. Derating the engine to 2.3 kWe or using carbon grid materials yields a substantial increase in service life. Using the probabilistic model to study driver sensitivities shows that uncertainties about eroded area fraction, net sputter yield and impingement current fraction in space are the major risk drivers. Efforts to obtain more information about these drivers have been initiated, as well as the development of improved engine designs centering on the use of carbon materials and changes in ion optics and engine configuration.

Acknowledgements

The research described in this paper was conducted at the Jet Propulsion Laboratory, California Institute of Technology, and was sponsored by the National Aeronautics and Space Administration.

References

[1] J.M. Monheiser and P.J. Wilbur. Effects of Design and Operating Conditions on Accelerator-Grid Impingement Current. In 23^{rd} *International Electric Propulsion Conference*, Seattle, WA, 1993. AIAA-93-174.

[2] X. Peng, W. M. Ruyten, and D. Keefer. Three-Dimensional Particle Simulation of Grid Erosion in Ion Thrusters. In 22^{nd} *International Electric Propulsion Conference*, Viareggio, Italy, 1991. AIAA-91-119.

[3] X. Peng, Will. Ruyten, and D. Keefer. Charge-Exchange Grid Erosion Study for Ground-Based and Space-Based Operations of Ion Thrusters. In 23^{rd} *International Electric Propulsion Conference*, Seattle, WA, 1993. AIAA-93-173.

[4] X. Peng, W.M. Ruyten, and D. Keefer. Monte Carlo Simulation of Ion-Neutral Charge Exchange Collisions and Grid Erosion in an Ion Thruster. In 29^{th} *Aerospace Sciences Meeting*, Reno, NV, 1991. AIAA-91-0607.

[5] J.R. Brophy, L.C. Pless, and J. E. Polk. Test-to-Failure of a Two-Grid 30-cm Dia. Ion Accelerator System. In 23^{rd} *International Electric Propulsion Conference*, Seattle, WA, 1993. AIAA-93-172.

[6] G.K. Wehner and 1). Rosenberg. Angular Distribution of Sputtered Material. *J. Appl. Phys.*, 31(1):177- 179, 1960.

[7] 1). Rosenberg and G.K. Wehner. Sputtering Yields for Low Energy He^+, Kr^+, and Xe^+ Ion Bombardment. *J. Appl. Phys.*, 33(5) :1842- 1845, 1962.

[8] N.R. Moore, 1). Ebbeler, and M. Creager. An Improved Approach for Flight Readiness Assessment- Probabilistic Models for Flaw Propagation and Turbine Blade Fatigue Failure. Technical Report 92-32, Jet Propulsion Laboratory, California Institute of Technology, Pasadena, CA, 1992.

[9] N. Moore, D. Ebbeler, and M. Creager. Probabilistic Service Life Assessment. In *Reliability Technology- 1992*, volume AD-28. American Society of Mechanical Engineers, 1992. ISBN 0 7918-1095-X.

[10] N .R. Moore, D. Ebbeler, and M. Creager. An Improved Approach for Flight Readiness Assessment- Methodology for Failure Risk Assessment and Application Examples. Technical Report 92-15, Jet Propulsion Laboratory, California Institute of Technology, Pasadena, CA, 1992.

[11] N . Moore, D. Ebbeler, and M . Creager. A Methodology for Probabilistic Prediction of Structural Failures of Launch Vehicle Propulsion Systems. In 31*st* *Structures,Structural l)y?/(I?)/-ics and Materials Conference*, pages 1092- 1104, 1990. 90-1140-CP.

[12] H.O. Madsen, S. Krenk, and N.C. Lind. *Methods of Structural Safety*. Prentice Hall, Englewood Cliffs, New Jersey, 1986.

[13] M.J. Patterson and T.R. Verhey. 5kW Xenon Ion Thruster Lifetest. In 21*st* *International Electric Propulsion Conference*, Orlando, FL, 1990. AI AA-00-2543.

[14] M.J. Patterson and T. Haag. Performance of the 30-cm Lightweight Ion Thruster. In 23*rd* *International Electric Propulsion Conference*, Seattle, WA, 1993. AI AA-93-108.

[15] J .R. Brophy, L.C. Pless, J . Anderson, and J. Mueller. Operating Characteristics of a 15-cm Dia. Ion Engine for Small Planetary Spacecraft. In 23*rd* *International Electric Propulsion Conference*, Seattle, WA, 1993. AI AA-93-I 10.

[16] C.E. Garner, J .R. Brophy, and L.C. Pless. Fabrication and Testing of Carbon-Carbon Grids for Ion Engines. In 28*th* *Joint Propulsion Conference*, Nashville, TN, 1992. AI AA-92-3149.

17] J. Meserole and 1). Hedges. Comparison of Erosion Rates of Carbon-Carbon and Molybdenum Ion Optics. In 23*rd* *International Electric Propulsion Conference*, Seattle, WA, 1993. AI AA-93-111.

18] J. Mueller, D.K. Brown, C.E. Garner, and J.R. Brophy. Fabrication of Carbon-Carbon Grids for Ion Optics. In 23*rd* *International Electric Propulsion Conference*, Scattic, WA, 1993. AIAA-93-112.

[19] J. Blandino, Aug. 1993. Private communication.

[20] S . Kami, C. Dulgeroff, and R.T. Bechtel. Status of the J-Series 30-cm Mercury Ion Thruster. In 16*th* *International Electric Propulsion Conference*, New Orleans, LA, 1982. AIAA-82-1904.

[21] J. Bohdansky, J. Roth, and 11.1,. Bay. An Analytical Formula and Important Parameters for Low-Energy Ion Sputtering. *J. Appl. Phys.*, 51 (5):2861-2865, 1980.

[2'2] E. Hechtl and J. Bohdansky. Sputtering Behavior or Graphite and Molybdenum at Low Bombarding Energies. *Journal of Nuclear Materials*, 122 & 123:1431-1436, 1984.

[23] D.L. Youchison, M.D. Nahemow, R.T. McGrath, and A.J. Baratta. The Role of Surface Microstructure in the Sputtering of Graphite. *J. Vat. Sci. Technol.*, 9(3):753- 758, 1991.

[24] G.K. Wehner. Sputtering Yields for Normally Incident Hg^+ Ion Bombardment at Low Ion Energy. *Phys. Rev.*, 108(1):35 45, 1957.

[25] N. Laegreid and G.K. Wehner. Sputtering Yields of Metals for Ar^+ and Ne^+ ions with Energies from 50 to 600" eV. *J. Appl. Phys.*, 32(3):365 369, 1961.

[26] J.R.Brophy. A Segmented Ion Engine Design for Solar Electric Propulsion Systems. In *43rd Congress of the International Astronautical Federation*, Washington, D.C., 1992. IAF-92-0608.

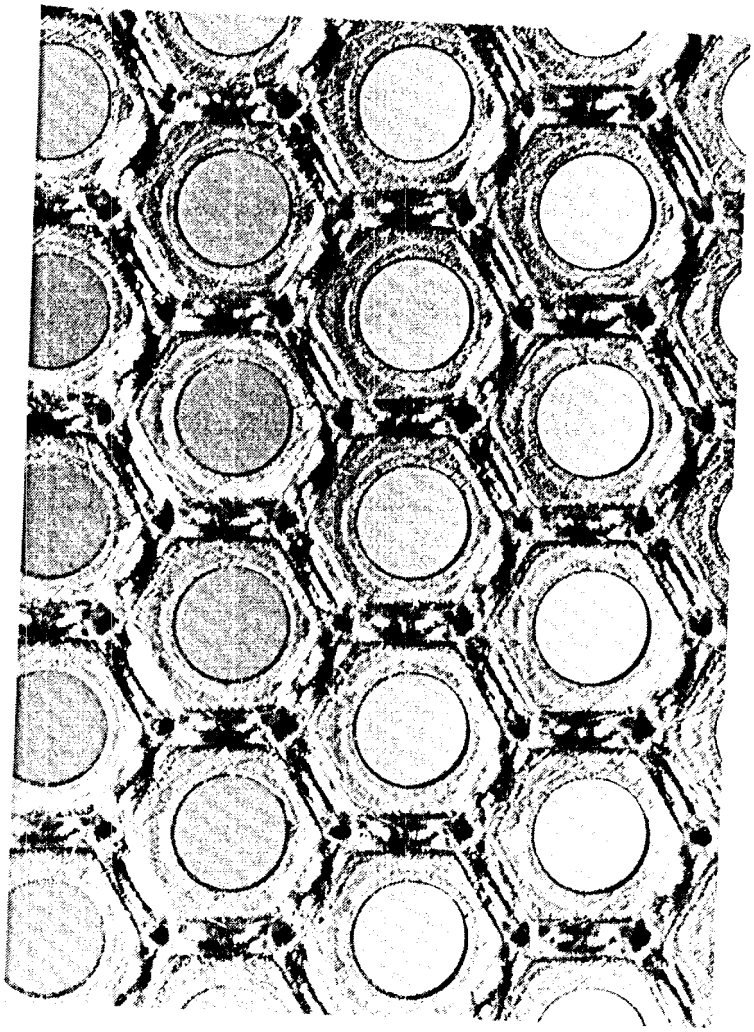

Fig 2

3 PROBABILISTIC FAILURE RISK ASSESSMENT

Information from experience can be combined with information from analytical modeling to estimate failure risk quantitatively using the approach shown in Figure 1. This approach is applied individually to those failure modes identified for analysis. Probabilistic failure modeling is based on available knowledge of the failure phenomenon and of such governing parameters as loads and material properties, and it provides the prior failure risk distribution of Figures 1 and 2. This prior distribution can be modified to reflect available success/failure data in a Bayesian statistical analysis. The probabilistic failure risk assessment approach shown in Figures 1 and 2 is discussed in detail by Moore, et al. (Dec., 1992; Nov., 1992; June, 1992; and 1990).

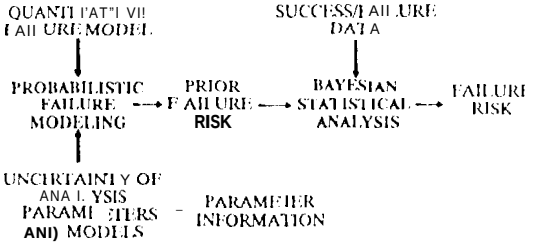

Fig. 3 Probabilistic failure risk assessment

Experience can include physical parameter information in addition to success/failure data. Information about physical parameters can be derived from measurements taken during tests or service, from analyses to bound or characterize parameter values, from applicable experience with similar systems, or from laboratory tests. Measurements of physical parameters used in analytical modeling, e.g., temperatures and loads, can be an important information source in failure risk assessment. Physical parameter information is incorporated into probabilistic failure modeling and is reflected in the prior failure risk distribution.

Success/failure data can be acquired from testing or service experience. The failure risk distribution resulting from the combination of the prior distribution and the success/failure data is the description of failure risk which is warranted by the information available. As additional information regarding governing physical parameters becomes available it can be incorporated into analytical modeling to obtain a revised prior failure risk distribution. Additional information in the form of success/failure data can be processed by the Bayesian statistical analysis of Figure 1 to update the prior failure risk distribution using the procedure given by Moore, et al. (June, 1992 and 1990).

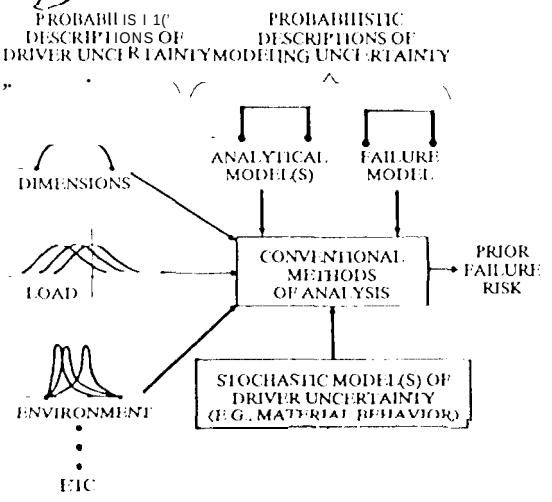

Fig. 4 Probabilistic failure modeling

The analysis procedures used in probabilistic failure modeling, shown in Figure 2, are directly derived from deterministic methods for analyses of failure modes which express failure parameters, such as burst pressure or fatigue life, as a function of governing parameters or drivers. For fatigue failure modes, the drivers include dimensions, loads, material behavior, model accuracy, and environmental parameters such as local temperatures. The accuracy of the models and procedures used in probabilistic failure modeling should be probabilistically described and treated as a driver. Probabilistic descriptions of model accuracy are based on experience in using the models and procedures, and when available, on tests conducted specifically to evaluate their accuracy.

A driver for which uncertainty is to be considered must be characterized by a probability distribution over the range of values it can assume. That distribution expresses uncertainty regarding specific driver values within the range of possible values. A driver probability distribution must represent both intrinsic variability of the driver and uncertain knowledge or limited information on which to base the driver characterization.